Comprehensive analysis of radiative cooling enabled thermoelectric energy harvesting

Journal of Physics: Photonics

PAPER

Comprehensive analysis of radiative cooling enabled thermoelectric energy harvesting

Yuxiao Zhu, Daniel W Newbrook, C H de Groot and Ruomeng Huang*

School of Electronics and Computer Science, University of Southampton, Southampton, United Kingdom
* Author to whom any correspondence should be addressed.

E-mail: r.huang@soton.ac.uk

Keywords: radiative cooling, thermoelectric generator, COMSOL, IoT

Supplementary material for this article is available online

OPEN ACCESS

RECEIVED
1 February 2023

REVISED
27 March 2023

ACCEPTED FOR PUBLICATION
3 April 2023

PUBLISHED
25 April 2023

Abstract

The market for Internet-of-things (IoT) with integrated wireless sensor networks is expanding at a rate never seen before. The thriving of IoT also brings an unprecedented demand for sustainable micro-Watt-scale power supplies. Radiative cooling (RC) can provide a continuous temperature difference which can be converted by a thermoelectric generator (TEG) into electrical power. This novel combination of RC with TEG expands the category of sustainable energy sources for energy harvesting. However, the further application of RC-TEG requires a holistic investigation of its RC-TEG performance which is dependent on many different parameters. Using 3D finite element method simulation, this works provides a comprehensive analysis of the concept of RC-TEG by investigating the impact of radiative cooler properties, TEG parameters, and environmental conditions, to provide a full picture of the performance of RC-TEG devices. The capability of RC-TEG to provide continuous power supply is tested using real-time environmental data from both Singapore and London on two different days of the year, demonstrating continuous power supply sufficient for a wide range of physical devices.

1. Introduction

Energy harvesting from a renewable source is a promising alternative for sustainable and clean power generation [1]. Many energy harvesting technologies (e.g. Photo-Voltaics, wind) have been developed in the past decades with massive effort devoted to pushing the conversion efficiency to its limit [2]. Exploring new renewable energy sources that expand the current energy harvesting portfolio will contribute significantly to our society's energy sustainability and the roadmap toward net-zero emission by 2050 [3]. Radiative cooling (RC) is a ubiquitous process by which a surface loses heat through thermal radiation. The significant temperature difference between the earth (around 300 K) and space (2.7 K) can potentially be utilised to cool the earth's surface by emitting thermal infrared radiation to space through the atmosphere [4, 5]. The high transmittance window in the atmosphere at a wavelength between 8 and 13 μm coincidentally matches well with the blackbody radiation from a 300 K object, making the concept of RC possible by avoiding radiation re-absorption.

Recent advances in this field have led to the awareness of RC as an essential technology for energy efficiency and harvesting applications. At first, RC applications were mainly focused on the night sky. Several works have achieved excellent cooling effects at night by optimizing materials [6] and coatings [7] on a RC surface. However, daytime RC proves difficult to achieve because the absorption from the highly intensive solar spectrum (0.3–3.0 μm) quickly exceeds the cooling energy [8]. In 2014, Raman *et al* achieved daytime RC for the first time by developing spectrally-selective filters with high emissivity within the atmospheric window but extremely low absorptivity in the solar spectrum [5]. Since then, more advancements have been made to improve the performance of RC through materials choice [9] and photonic structures [10], enabling applications in building-integrated cooling systems [11] and solar cell panel cooling [10, 12].

More recently, RC has been investigated to exploit its temperature difference for energy generation. And thermal energy can be converted into electricity by integrating thermoelectric generators (TEGs) [13, 14]. A TEG can harvest thermal energy into electrical energy based on the Seebeck effect [15]. It is formed by connecting an n-type semiconductor material electrically in series and thermally in parallel across a temperature gradient to a p-type semiconductor material, allowing current flow between the two. In addition, TEGs offer a maintenance-free solid-state operation with high lifetime reliability that often significantly exceeds those of the devices they power [14]. The concept of RC powered TEGs has since been developed as a stable, continuous power supply for several different applications. Compare with TEG with solar absorbers [16], integrating it with a radiative cooler has more advantages in continuous power generation. For example, Raman *et al* developed an RC-TEG that can work day and night continuously, generating a power of 25 mW m^{-2} [17]. Such power is sufficient for transmitting Bluetooth signals or other IoT work [18]. Zhan *et al* enhanced thermoelectric output power via RC using a novel nanoporous alumina film [19]. Several studies also focused on using RC in wearable TEGs [20] and achieved a power density of 55 mW m^{-2} at 293 K [21]. Xia *et al* developed a thin film RC-TEG that allowed 24 h continuous power generation [22]. Mu *et al* also studied thin film TEGs in combination with RC, achieving a continuous average 0.18 mV output for 24 h [23]. In addition, RC-TEG also possesses great potential to be implemented as wearable energy harvesting devices [24] and smart windows [25].

Several analytical studies were conducted to model and investigate the performance of RC-TEG. For example, Liu *et al* have modelled the RC-TEG device numerically and investigated the effects of different RC spectra and other relevant parameters on the RC-TEG device [26]. A mathematical modelling study of RC versus thermoelectric refrigerators was carried out by Liao *et al* [27]. Zhao *et al* also conducted mathematical modelling of the RC-TEG device, focusing on optimising the TEG parameters [28].

It is clear that a variety of parameters from both the radiative cooler and the TEG itself determines the performance of an RC-TEG. In addition, as a ubiquitous process, the power output is also highly dependent on its environmental conditions, as the atmospheric window transmittance can be affected by geographical location [29], cloud cover [30], and humidity conditions [31]. Such environmental variations can significantly impact the RC power and change the RC-TEG performance. However, despite the growing interest in this novel energy harvesting technology, a comprehensive investigation of its performance considering all parameters, to the best of our knowledge, is lacking. For example, environmental parameters (e.g. convection, water vapour) should be taken into account when optimising the RC-TEG. In addition, parameters in both the radiative cooler and the TEG should be optimised simultaneously [32]. Therefore, a holistic approach should be adopted concerning environmental and device parameters when investigating and optimising the RC-TEG performance.

This work provides a comprehensive investigation of the performance of RC-TEG using a 3D finite element analysis (FEM) modelling approach. The 3D FEM approach enables higher accuracy analytical modelling by considering not only RC performance, and TEG design but also environmental aspects such as atmosphere emissivity and air convection. These parameters are studied systematically to provide a complete picture of the performance of RC-TEG. The power generation capability of the RC-TEG is calculated using real-time solar irradiance and ambient temperature data in different cities to evaluate its performance in different regions on earth.

2. Method

Figure 1(a) shows the model of the RC-TEG developed in COMSOL in this work. A square radiative cooler with a width of W_{Cooler} is integrated on the top surface of the TEG model. It is exposed to the sky directly in the simulation. An insulating layer (quartz glass) with the same size is sandwiched between the radiative cooler and TEG. The bulk TEG model contains eight N/P-leg pairs where the width and height of both legs are kept the same as W_{TE} and H_{TE}, respectively, in this work. The N/P legs are connected in series by copper interconnects. The electrical contact resistance is also considered in the model by including a 10^{-8} Ω m^2 contact resistivity at each copper/thermoelectric leg interface. The thermoelectric materials used in this work are $Bi_2Te_{2.7}Se_{0.3}$ for the N-type leg and BiSbTe for the P-type leg. The detailed thermoelectric properties, such as the Seebeck coefficient, electrical and thermal conductivities, and figure of merit (ZT) values of both materials, are adopted from past studies [33, 34] and presented in figures 1(b)–(e). The ambient temperature is set at 293.15 K as default in all simulations unless otherwise specified. During simulation, the TEG is virtually connected with an external load to form a circuit. The inlet and outlet of the copper interconnect serve as a terminal (variable V) and the ground ($V = 0$ V) for the model. The resistance of the external load is swept to reach the maximum power density (PD_{max}), as exemplified in figure S1. More details of the simulation can be found in the support information.

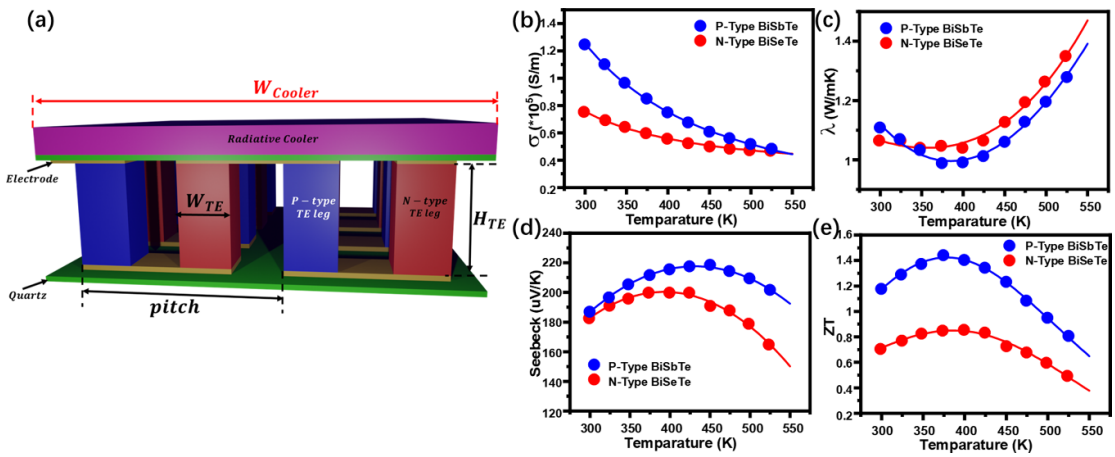

Figure 1. Schematic and temperature-dependent material properties of the N-type and P-type thermoelectric materials used in our RC-TEG model. (a) Schematic, (b) electrical conductivity, (c) thermal conductivity, (d) Seebeck coefficient, and (e) ZT [33, 34].

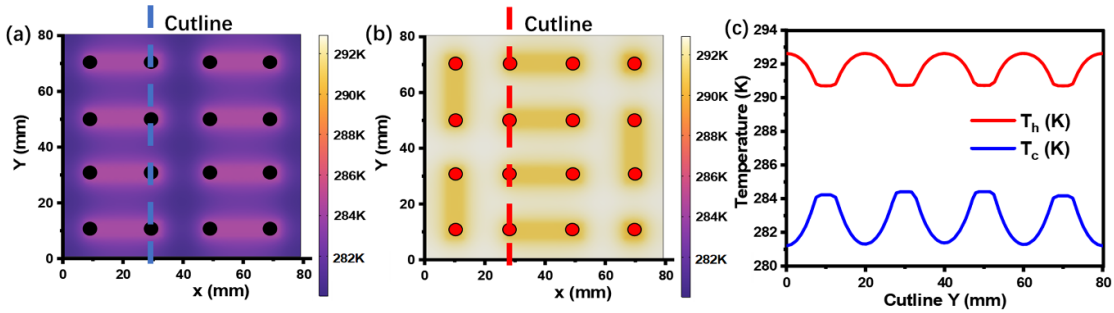

Figure 2. Temperature profile of the RC-TEG under typical working conditions. (a) Exposed radiative surface (b) shielded counter surface. The dots represent the locations where the average temperature readings are used to define T_c and T_h. (c) The temperature distribution at the cutlines in (a) and (b).

In the RC part, the RC power P_{cool} can be expressed as [5]:

$$P_{cool} = P_{rad} - P_{atm} - P_{sun} - P_{non\text{-}rad} \quad (1)$$

where P_{rad} is the thermal radiation, P_{atm} is the absorbed atmospheric radiation, $P_{non\text{-}rad}$ is the intrinsic cooling loss, and P_{sun} is the absorbed solar radiation. Each term in equation (1) is integrated across a full electromagnetic spectrum. This work will focus mainly on the emissivity in the solar band (0.3–2.5 μm) and the radiation band (8–13 μm). The emissivity of the band (2.5–8 μm) is fixed at 0 unless otherwise specified. The solar irradiance is set to 1000 W m^{-2} in the simulation unless otherwise specified. When exposing the radiative cooler to the sky, the temperature of the top surface will drop, creating a temperature difference ΔT between the top and bottom surfaces. However, the temperature is not uniformly distributed on both surfaces due to the direct contact with the TEG. For example, figure 2 presents the temperature profiles on both surfaces under one simulation condition. It is clear that the temperature directly on top of a TEG leg is slightly higher on the top (cold) surface than the surrounding areas (figure 2(a)). On the contrary, the temperature directly below a TEG is slightly colder on the bottom (hot) surface than its surroundings (figure 2(b)). In this work, we define the top side (hot) temperature T_h as the average temperature of the 16 points above the TEG legs and the bottom (cold) side temperature T_c as the average temperature of the 16 points below the TEG legs. The temperature difference is ΔT, defined as $\Delta T = T_h - T_c$. This provides us with a better understanding of the actual temperature gradients over the TEG as the distribution of the temperature is not uniform across the surfaces (figure 2(c)). The non-uniformity is caused by the limited thermal conductivity of the insulating layer of quartz glass used between the cooler and the TEG in this work. We have conducted simulations concerning the impact of different thermal conductivity of the insulating material. As shown in figure S2, increasing the thermal conductivity results in higher ΔT. This increment saturates when the thermal conductivity reaches *ca.* 500 W mK^{-1}. This suggests the uneven temperature distribution can be mitigated by adopting insulating layers with higher thermal conductivity, leading to a

more uniform temperature profile and higher ΔT. In addition to the thermal conduction, the heat exchange of RC-TEG with the environment is also considered by defining convections for both the top surface ($Conv_T$) and bottom surface ($Conv_B$). All simulations are carried out on the COMSOL platform with the thermal transfer process set as a steady-state condition.

3. Results and discussion

3.1. RC-TEG performance under different convections

An RC-TEG functions when RC generates a temperature difference between the top and bottom surfaces. Heat exchange with the atmosphere through convection plays an essential role in the temperature profile of the RC-TEG. Figures 3(a) and (b) illustrate the variation of both T_c and T_h under different convection conditions. Both T_c and T_h increase with increasing convections at both surfaces. This is unsurprising as the environmental temperature is set as 293.15 K in this work. Higher convection will facilitate the heat exchange between the RC-TEG and the atmosphere, leading to higher temperatures close to the environment. Achieving a more significant ΔT, therefore, requires different convection conditions for each surface, as shown in figure 3(c). Convection at the top surface should be minimised to retain the low temperature generated by RC while the convection at the bottom surface should be promoted. In this set of simulations, the largest ΔT of 7.3 K is obtained when $Conv_T$ is as low as 1 W $m^{-2}K^{-1}$ while $Conv_B$ is 100 W $m^{-2}K^{-1}$. It is also evident that the impact of $Conv_T$ is much more significant than $Conv_B$, with ΔT quickly deteriorating to 3.5 K when $Conv_T$ increases to 10 W $m^{-2}K^{-1}$. The associated power performance of RC-TEG is shown in figure 3(d). As expected, the higher power output takes place at the largest ΔT, reaching over 200 mW m^{-2}. However, such high power output would be halved if the $Conv_T$ increases from 1 W $m^{-2}K^{-1}$ to 4 W $m^{-2}K^{-1}$. At a $Conv_T$ of 10 W $m^{-2}K^{-1}$, the output power will drop to below 50 mW m^{-2}. It is, therefore, key for RC-TEG to keep good thermal insulation to the environment to minimise heat exchange. Several experimental RC-TEG works to achieve that by enclosing the radiative cooler within a vacuum chamber [26]. In the following simulations, we will set $Conv_T$ and $Conv_B$ to 1 W $m^{-2}K^{-1}$ and 50 W $m^{-2}K^{-1}$, respectively.

3.2. RC-TEG performance under different atmosphere emissivity

We will now investigate the impact of atmospheric emissivity on RC-TEG performance. The atmospheric emissivity depends on the concentration of water vapour, CO_2, CO and other gas in the air [35]. In particular, water vapour absorption dominates the atmospheric absorptance within the atmospheric window; the transparency of the sky is sensitive to precipitable water vapour concentration, which is correlated with relative humidity and ground temperature, and thus varies geographically [36]. Higher humidity in the air could lead to high atmosphere emissivity in the 8–13 μm band, which directly affects RC-TEG performance. Figure 4 demonstrates the effect of atmospheric emissivity on the performance of RC-TEG. As the atmospheric emissivity increases from 0 to 0.5, the ΔT decreases by about 5°. Such decrement is due to the fact that more power is absorbed by the atmosphere rather than radiated to the colder outer space, leading to inferior power generation from the RC-TEG model. This trend proves that the RC-TEG performance is strongly dependent on the weather. Under a clear sky and dry atmosphere where the atmospheric emissivity is low (<0.3), the RC-TEG model is capable of producing a continuous power of over 150 mW m^{-2}. However, this drops very quickly to below 100 mW m^{-2} when the sky is overcast with high humidity. In subsequent model simulations, the atmospheric emissivity was maintained at 0.3 for all 8–13 μm and 1 for the other bands 0–8 μm and 13–25 μm.

3.3. RC-TEG performance under different radiative cooler emissivity

As an essential part of the RC-TEG, the emissivity (ε) of the radiative cooler is crucial to the power performance of the device. In this work, we mainly focused on studying the impact of emissivity in two bands of 0.3–2.5 μm and 8–13 μm. The former band decides how much solar energy is absorbed by the radiative cooler. This is especially important for daytime RC. The latter band in the atmospheric window of 8–13 μm determines the cooling power achieved by the radiative cooler. Figure 5(a) presents the effect of surface emissivity on the temperature difference ΔT of an RC-TEG device in the daytime. A positive ΔT indicates that the top surface is colder than the bottom surface and that the cooling power is dominating the temperature profile of our RC-TEG. A cooler with a larger $\varepsilon_{8–13\ \mu m}$ can generate more cooling power, leading to larger ΔT. However, positive ΔT only prevails when the $\varepsilon_{0.3–2.5\ \mu m}$ is maintained at a low level. Increasing $\varepsilon_{0.3–2.5\ \mu m}$ can result in the top surface being heated up by absorbing solar energy, cancelling out the positive ΔT from RC. When the heat absorbed from solar irradiation outweighs the heat dissipated via RC, the temperature difference ΔT becomes negative, and the radiative cooler effectively turns into a heat absorber. The power performance of the RC-TEG under different surface emissivity scenarios is shown in figure 5(b). Under minor $\varepsilon_{0.3–2.5\ \mu m}$ conditions, the output power increases with increasing $\varepsilon_{8–13\ \mu m}$ values as the ΔT

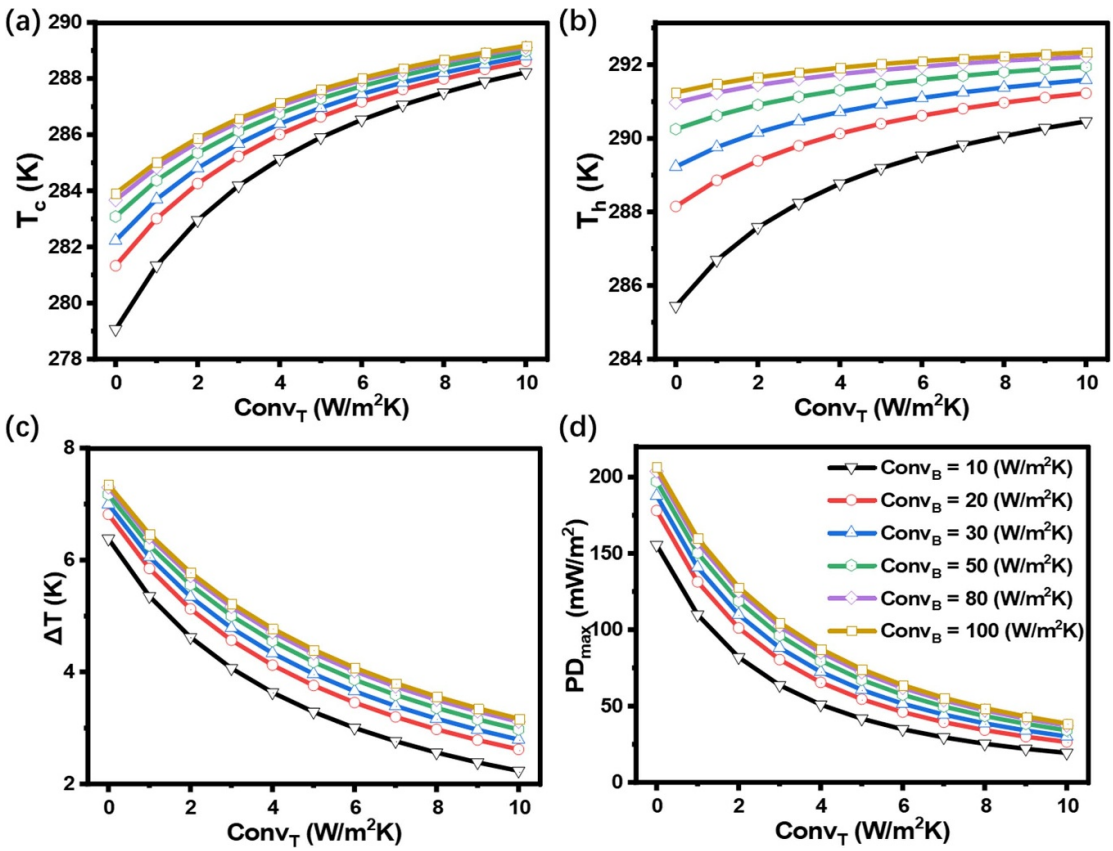

Figure 3. FEM simulation performance of RC-TEG under various top surface convection ($Conv_T$) and bottom surface convection ($Conv_B$) conditions. (a) Top and (b) bottom surface temperature, (c) the temperature difference between the top and bottom surface (ΔT), (d) the power density (PD_{max}). Other simulation parameters were fixed at $W_{Cooler} = 80$ mm, $W_{TE} = 5$ mm, $H_{TE} = 10$ mm, and pitch = 40 mm.

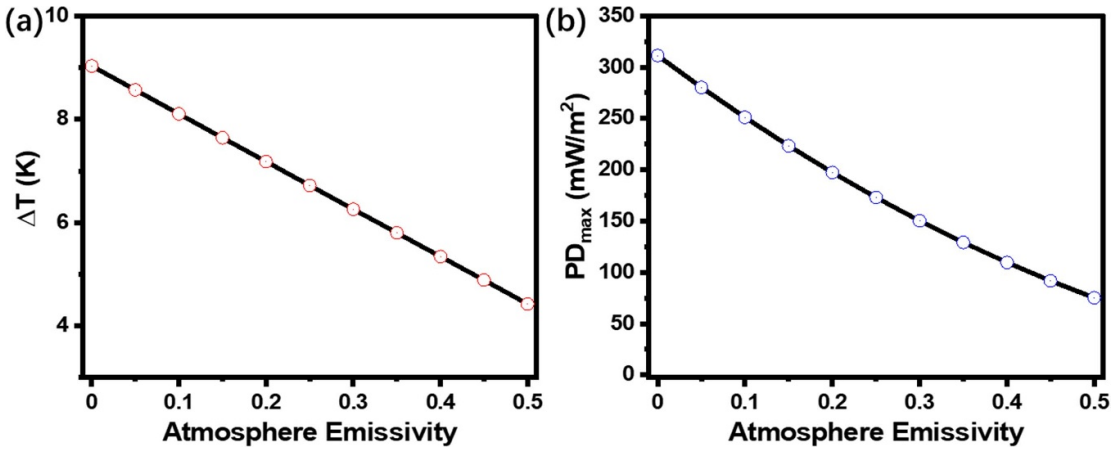

Figure 4. Performance of RC-TEG obtained in COMSOL simulation as a function of atmosphere emissivity (a) temperature difference (ΔT) and (b) power density (PD_{max}). Other simulation parameters were fixed at $W_{Cooler} = 80$ mm, $W_{TE} = 5$ mm, $H_{TE} = 10$ mm, and pitch = 40 mm.

increases with more cooling power. However, in the case of a large $\varepsilon_{0.3–2.5\ \mu m}$ (e.g. 0.05), RC-TEG can also generate power even when $\varepsilon_{8–13\ \mu m}$ is small, except that the device is now operating as a solar-absorber TEG under such conditions. The amount of power attenuates to zero with increasing $\varepsilon_{8–13\ \mu m}$ value as the cooling power slowly cancels out the solar energy and rises again as the ΔT becomes positive. It is clear that $\varepsilon_{0.3–2.5\ \mu m}$ of the cooler needs to be as small as possible to avoid the negative influence of solar energy, while the $\varepsilon_{8–13\ \mu m}$ must be as large as possible to ensure a continuous power supply from RC-TEG.

We also investigate the impact from the band between 2.5 and 8 μm while keeping the $\varepsilon_{8–13\ \mu m}$ to be 1 and $\varepsilon_{0.3–2.5\ \mu m}$ to be 0 as shown in figure S3. In this work, the temperature of our radiative cooler is always

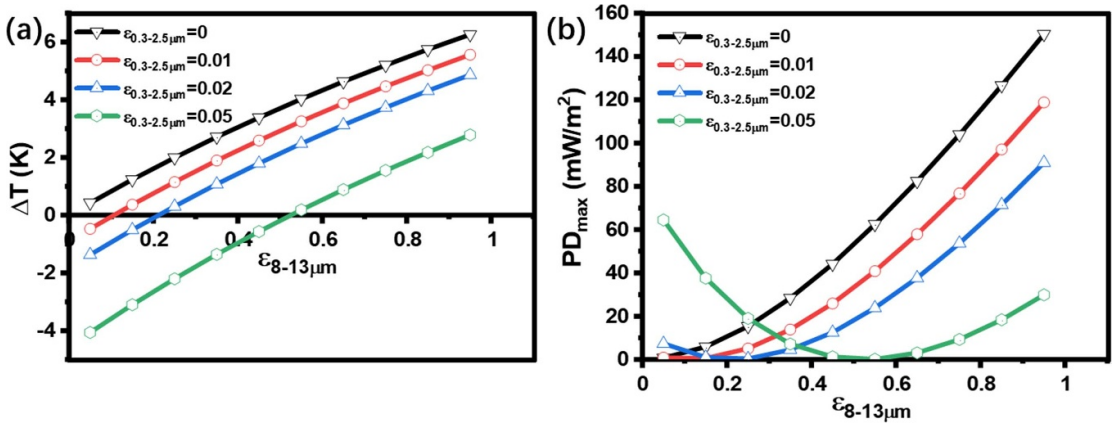

Figure 5. Performance of RC-TEG as a function of emissivity in the solar and thermal IR spectrum. (a) Temperature difference (ΔT) (b) power density (PD_{max}) obtained from COMSOL simulation as a function of 8–13 μm ($\varepsilon_{8-13\ \mu m}$) and 0.3–2.5 μm ($\varepsilon_{0.3-2.5\ \mu m}$) surface emissivity. Other simulation parameters were fixed at $W_{Cooler} = 80$ mm, $W_{TE} = 5$ mm, $H_{TE} = 10$ mm, and pitch = 40 mm.

lower than that of the atmosphere. If the RC emissivity in the 2.5–8 μm band is larger than 0, the atmosphere will always radiate energy to the RC (as there is no atmospheric window within this band for the energy to be radiated to the space). This will increase the temperature of the RC and decrease the temperature difference (shown in figure S3(a)) as well as the power performance of the RC-TEG (shown in figure S3(b)).

3.4. RC-TEG performance with different TE parameters

The geometrical parameters of the RC-TEG also play a vital role in the power performance. Here we will mainly focus on the impact of the TEG pitch and the width of the radiative cooler W_{Cooler} while keeping the leg width W_{TE} constant. Figure 6 depicts the effect on RC-TEG performance when both W_{Cooler} and pitch are varied. It is worth mentioning that the starting point of W_{Cooler} is limited by the pitch size and is, therefore, different in each case. It can be observed in figure 6(a) that ΔT firstly increases with increasing W_{Cooler}. This is reasonable as larger radiative coolers can generate more cooling power, leading to a colder top surface. However, such an increase quickly saturates at a larger W_{Cooler} if the TEG pitch remains unchanged, as the cooling on top of the TEG area is limited by the heat conduction on the radiative cooler (shown in figure S4). A further increase of the cooling power from the radiative cooler cannot further reduce the cold side temperature. On the other hand, enlarging the TEG footprint under the radiative cooler by increasing its pitch facilitates thermal conduction on the radiative cooler at the TEG leg areas (shown in figure S5), leading to improved ΔT and TEG output power, as shown in figures 6(a) and (b). It should be noted here that figure 6(b) only considers the absolute power output, the change of radiative cooler size also affects the power density (PD_{max}) of the device, which is plotted in figure 6(c). As PD_{max} is also a function of the device area, it firstly increases with increasing power and subsequently decreases as the power saturates. Therefore, we can identify the optimised PD_{max} and W_{Cooler} for TEG with different pitch sizes, as shown in figure 6(d). It can be observed that the optimised PD_{max} and W_{Cooler} will increase with increasing TEG pitch.

We now focus on the scenario where the size of the radiative cooler is fixed and investigate the performance of RC-TEG under different TEG parameters. Figure 7 shows the effect on the RC-TEG of changing W_{TE} and H_{TE} while keeping the W_{Cooler} unchanged. It can be observed that increasing W_{TE} could lead to a decrease of ΔT (figure 7(a)). This is because when the W_{TE} is increasing, the thermal resistance of TEG will decrease, leading to smaller ΔT across the top and bottom sides. On the other hand, increasing H_{TE} increases the thermal resistance, resulting in larger ΔT. Figure 7(b) shows the results of PD_{max} as a function of W_{TE} and H_{TE}. It can be seen that when the H_{TE} is relatively small ($\leqslant$15 mm), the PD_{max} decreases as the W_{TE} increases. This is in line with the reduction of ΔT. Whereas at more significant H_{TE} conditions, a slight increase of PD_{max} can be noticed before it falls again with increasing W_{TE}. It is because the negative impact from considerable electrical resistance outweighs the gain from larger ΔT at small W_{TE} and large H_{TE}. An optimised set of TEG parameters can therefore be identified to reach the highest PD_{max}.

3.5. RC-TEG performance under real-time data

One of the key advantages of RC-TEG is its capability to provide a continuous power supply. However, the variation of environmental conditions at different times of day, days of the year, and geographical locations will all affect the power generation of an RC-TEG. Therefore, evaluating the power performance under

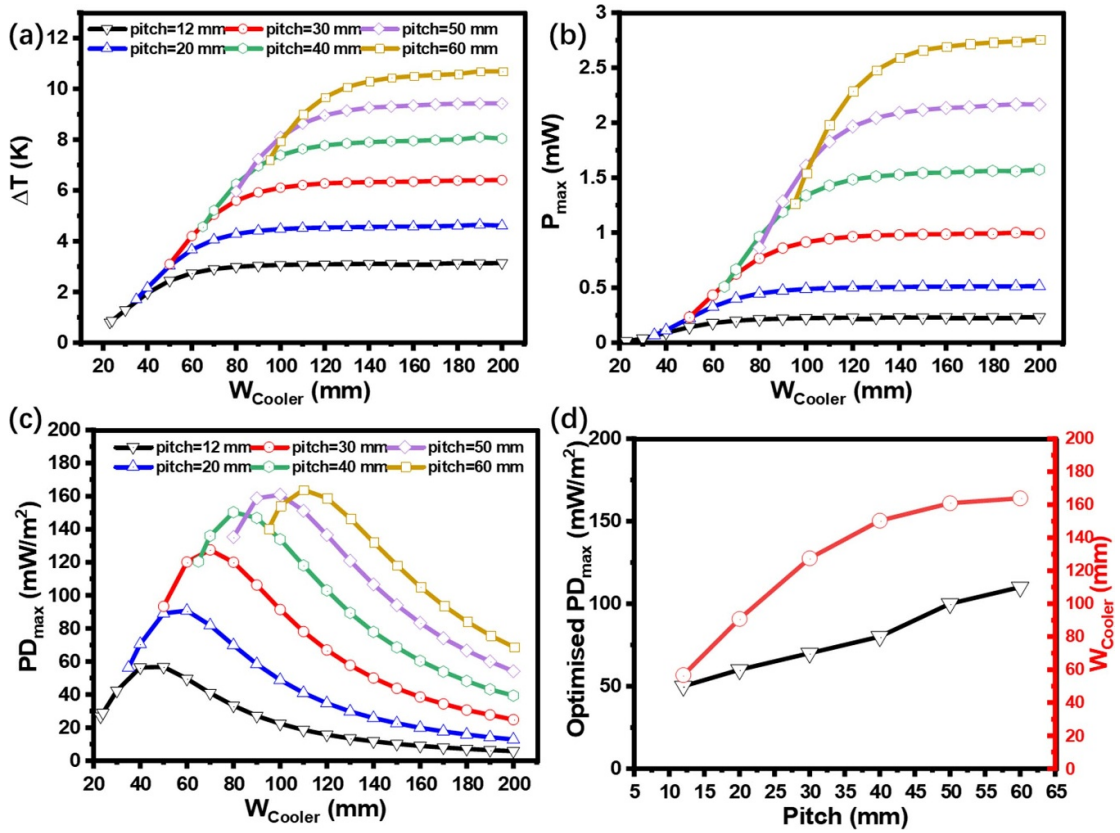

Figure 6. (a) Temperature difference, (b) power (P_{max}), (c) power density (PD_{max}) obtained from COMSOL simulation as a function of pitch and W_{Cooler}. (d) Optimised power density of W_{Cooler} on different pitches. Other simulation parameters were fixed at $W_{TE} = 5$ mm and $H_{TE} = 10$ mm.

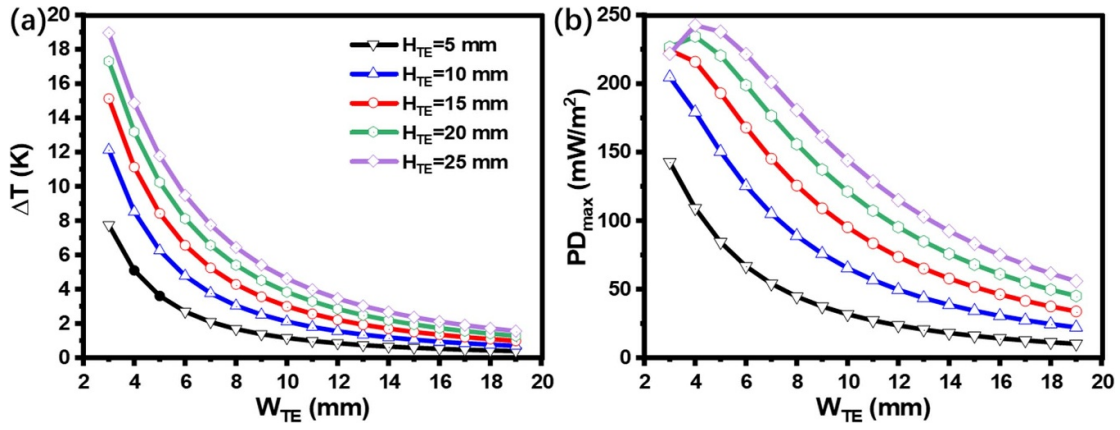

Figure 7. (a) Temperature difference, (b) PD_{max} obtained from COMSOL simulation as a function of H_{TE} and W_{TE}. Other simulation parameters were fixed at $W_{Cooler} = 120$ mm and pitch = 40 mm.

real-time environmental data is essential. In this work, we selected London and Singapore as two locations and investigated the full-day RC-TEG performance in summer (July 2021) and winter (January 2021) using real-time data, obtained from Prediction of Worldwide Energy Resources [37]. It is worth mentioning that all chosen days had similar weather (sunny) to minimise the influence of different atmospheric parameters on the simulation. The average solar irradiance of the two regions can be found in figure S6. Figure 8(a) shows the real-time temperature on the two days in London and Singapore, where significant differences between different days and locations can be observed. As a place near the equator, the temperatures of those two days in Singapore were similar at over 25 °C. On the other hand, temperatures in London were much lower and featured more considerable differences between summer and winter. Similarly, the solar irradiances in

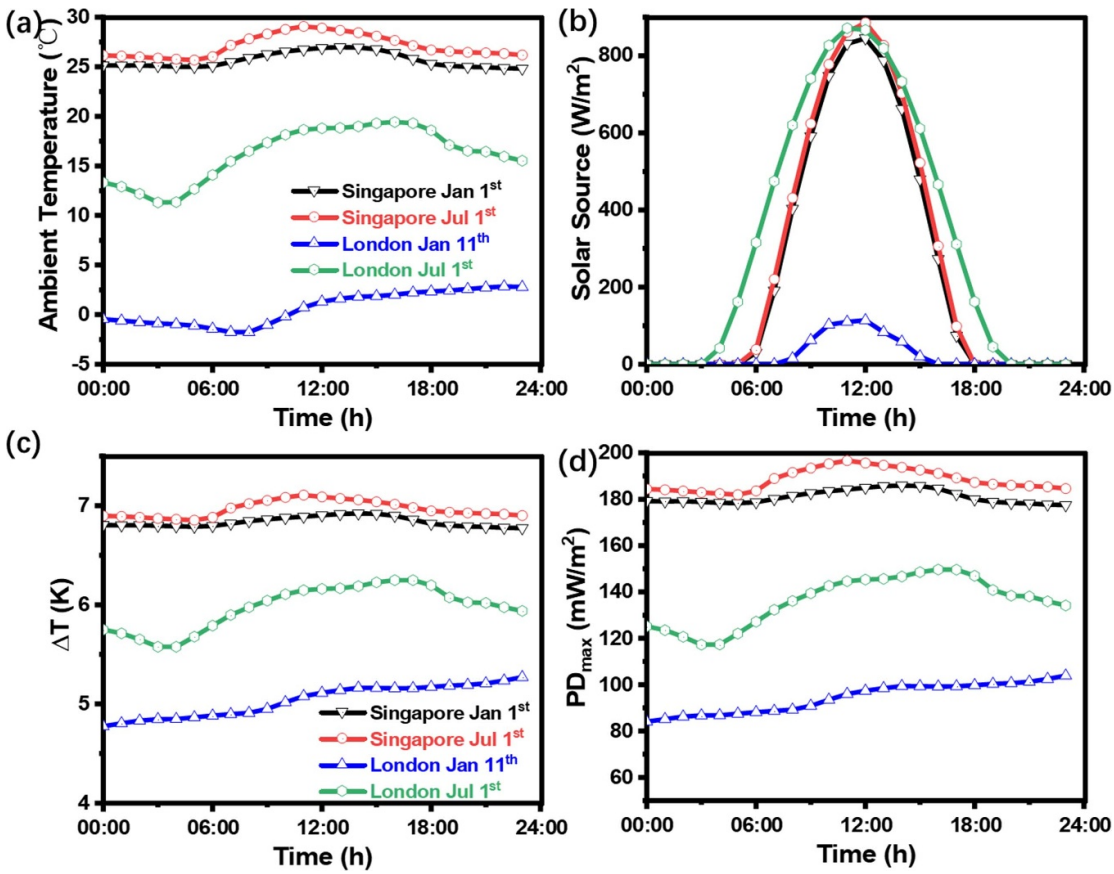

Figure 8. (a) Real-time temperature and (b) solar irradiance of London on 1 July 2021, 11 January 2021, Singapore on 1 July 2021, and 1 January 2021. (c) Temperature difference, (d) power density (PD_{max}) obtained from real-time data simulation. Other simulation parameters were fixed at $W_{Cooler} = 80$ mm, $W_{TE} = 5$ mm, $H_{TE} = 10$ mm, and pitch = 40 mm. Data obtained from Prediction of Worldwide Energy Resources (POWER NASA).

Singapore were also very close in those two days. However, they were quite different in the UK, both in the maximum irradiation power and duration.

Figure 8(c) presents the temperature difference ΔT across our RC-TEG under those real-time environmental conditions. A continuous positive ΔT can be achieved in all four conditions, indicating that the radiative cooler can provide unintermittent cooling power to the device throughout the day. The amplitude of the ΔT is strongly related to the real-time temperature as higher ambient temperature could increase the hot (bottom) side temperature of RC-TEG. The power performance of the RC-TEG under these conditions is shown in figure 8(d). The device can produce a continuous power supply in all four scenarios. Both days in Singapore feature average power of over 180 mW m^{-2}. The summer day in London also produces an average power of *ca.* 130 mW m^{-2}. Even on a cold winter day, an average power of over 90 mW m^{-2} can be achieved, sufficient enough to power a wide range of IoT and sensory devices [38].

4. Conclusions

This work provides a systematic analysis of TEGs driven by radiation cooling. The impacts from the environmental conditions, radiative cooler properties, as well as the TEG parameters were investigated to provide a complete picture of the performance dependence for RC-TEG devices. It was revealed that a thermally insulating top surface with low convection is crucial for RC-TEG to maintain a decent temperature difference for power generation. The atmosphere emissivity, related to the concentration of water vapour and other gases in the air, can also significantly affect the power output. From the perspective of the radiative cooler, whilst a high emissivity within the atmospheric window should be targeted for better power performance, the emissivity within the solar spectrum should be minimised to avoid heat absorption if continuous power generation is required. In addition, we have also revealed that the TEG parameters, including the area ratio between cooler and TEG, and the width and height of the TE legs, should be optimised for improved RC-TEG performance. In addition, the capability of RC-TEG to provide continuous power supply is tested using real-time environmental data from both Singapore and London on two different

days of the year, demonstrating continuous power supply in all four scenarios. Such real-time power generation performance has certain points towards the future application of RC-TEG in providing continuous power to a wide range of physical devices.

Data availability statement

All data supporting this study are available from the University of Southampton repository at DOI: https://doi.org/10.5258/SOTON/D2589.

Acknowledgments

This work was supported by an EPSRC Impact Acceleration Accounts Award, and the EPSRC ADEPT Programme Grant (EP/N035437/1). The authors acknowledge using the IRIDIS High-Performance Computing Facility and associated support services at the University of Southampton to complete this work.

ORCID iDs

Yuxiao Zhu https://orcid.org/0000-0003-1867-2297
Daniel W Newbrook https://orcid.org/0000-0002-5047-6168
C H de Groot https://orcid.org/0000-0002-3850-7101
Ruomeng Huang https://orcid.org/0000-0003-1185-635X

References

[1] Zhao B, Hu M, Ao X, Chen N and Pei G 2019 Radiative cooling: a review of fundamentals, materials, applications, and prospects *Appl. Energy* **236** 489–513
[2] Khare V, Nema S and Baredar P 2016 Solar-wind hybrid renewable energy system: a review *Renew. Sustain. Energy Rev.* **58** 23–33
[3] Luo Y and Kim C N 2019 Effects of the cross-sectional area ratios and contact resistance on the performance of a cascaded thermoelectric generator *Int. J. Energy Res.* **43** 2172–87
[4] Chen Z, Zhu L, Li W and Fan S 2019 Simultaneously and synergistically harvest energy from the sun and outer space *Joule* **3** 101–10
[5] Raman A P, Anoma M A, Zhu L, Rephaeli E and Fan S 2014 Passive radiative cooling below ambient air temperature under direct sunlight *Nature* **515** 540–4
[6] Catalanotti S, Cuomo V, Piro G, Ruggi D, Silvestrini V and Troise G 1975 The radiative cooling of selective surfaces *Sol. Energy* **17** 83–89
[7] Granqvist C G and Hjortsberg A 1980 Surfaces for radiative cooling: silicon monoxide films on aluminum *Appl. Phys. Lett.* **36** 139–41
[8] Hamza H A, Taha I and Ismail I 1995 Cooling of water flowing through a night sky radiator *Sol. Energy* **55** 235–53
[9] Zhai Y, Ma Y, David S N, Zhao D, Lou R, Tan G, Yang R and Yin X 2017 Scalable-manufactured randomized glass-polymer hybrid metamaterial for daytime radiative cooling *Science* **355** 1062–6
[10] Rephaeli E, Raman A and Fan S 2013 Ultrabroadband photonic structures to achieve high-performance daytime radiative cooling *Nano Lett.* **13** 1457–61
[11] Zhao B, Hu M, Ao X, Chen N, Xuan Q, Su Y and Pei G 2019 A novel strategy for a building-integrated diurnal photovoltaic and all-day radiative cooling system *Energy* **183** 892–900
[12] Zhu L, Raman A, Wang K X, Anoma M A and Fan S 2014 Radiative cooling of solar cells *Optica* **1** 32
[13] Zhu X, Blanco E, Bhatti M and Borrion A 2020 *Sci. Total Environ.* **757** 143747
[14] Snyder G J and Ursell T S 2003 Thermoelectric efficiency and compatibility *Phys. Rev. Lett.* **91** 148301
[15] Hamid Elsheikh M, Shnawah D A, Sabri M F M, Said S B M, Haji Hassan M, Ali Bashir M B and Mohamad M 2014 A review on thermoelectric renewable energy: principle parameters that affect their performance *Renew. Sustain. Energy Rev.* **30** 337–55
[16] Chowdhary A K, Reddy V A and Sikdar D 2022 Nanophotonics-enabled high-efficiency selective solar absorbers for waste heat management *IEEE Trans. Nanotechnol.* **21** 131–6
[17] Raman A P, Li W and Fan S 2019 Generating light from darkness *Joule* **3** 2679–86
[18] Haras M and Skotnicki T 2018 Thermoelectricity for IoT—a review *Nano Energy* **54** 461–76
[19] Zhan Z, ElKabbash M, Li Z, Li X, Zhang J, Rutledge J, Singh S and Guo C 2019 Enhancing thermoelectric output power via radiative cooling with nanoporous alumina *Nano Energy* **65** 104060
[20] Khan S, Kim J, Roh K, Park G and Kim W 2021 High power density of radiative-cooled compact thermoelectric generator based on body heat harvesting *Nano Energy* **87** 106180
[21] Liu Y *et al* 2022 Passive radiative cooling enables improved performance in wearable thermoelectric generators *Small* **18** 1–8
[22] Xia Z, Zhang Z, Meng Z, Ding L and Yu Z 2019 Thermoelectric generator using space cold source *ACS Appl. Mater. Interfaces* **11** 33941–5
[23] Mu E, Wu Z, Wu Z, Chen X, Liu Y, Fu X and Hu Z 2019 A novel self-powering ultrathin TEG device based on micro/nano emitter for radiative cooling *Nano Energy* **55** 494–500
[24] Liang J, Huang M, Zhang X and Wan C 2022 Structural design for wearable self-powered thermoelectric modules with efficient temperature difference utilization and high normalized maximum power density *Appl. Energy* **327** 120067
[25] Chowdhary A K and Sikdar D 2021 Design of electrotunable all-weather smart windows *Sol. Energy Mater. Sol. Cells* **222** 110921
[26] Liu J, Zhang J, Yuan J, Zhang D, Xing J and Zhou Z 2021 Model development and performance evaluation of thermoelectric and radiative cooling module to achieve all-day power generation *Sol. Energy Mater. Sol. Cells* **220** 110855
[27] Liao T, Xu Q, Dai Y, Cheng C, He Q and Ni M 2022 Radiative cooling-assisted thermoelectric refrigeration and power systems: coupling properties and parametric optimization *Energy* **242** 122546

[28] Zhao B, Pei G and Raman A P 2020 Modeling and optimization of radiative cooling based thermoelectric generators *Appl. Phys. Lett.* **117** 163903
[29] Hossain M M and Gu M 2016 Radiative cooling: principles, progress, and potentials *Adv. Sci.* **3** 1–10
[30] Kimball B A, Idso S B and Aase J K 1982 A model of thermal radiation from partly cloudy and overcast skies *Water Resour. Res.* **18** 931–6
[31] Khedari J, Waewsak J, Thepa S and Hirunlabh J 2000 Field investigation of night radiation cooling under tropical climate *Renew. Energy* **20** 183–93
[32] Zhou L *et al* 2022 Radiative cooling for energy sustainability: materials, systems, and applications *Phys. Rev. Mater.* **6** 1–22
[33] Yan X, Poudel B, Ma Y, Liu W S, Joshi G, Wang H, Lan Y, Wang D, Chen G and Ren Z F 2010 Experimental studies on anisotropic thermoelectric properties and structures of n-type $Bi_2Te_{2.7}Se_{0.3}$ *Nano Lett.* **10** 3373–8
[34] Poudel B *et al* 2008 High-thermoelectric performance of nanostructured bismuth antimony telluride bulk alloys *Science* **320** 634–8
[35] Wei P S, Chiu H-H, Hsieh Y-C, Yen D-L, Lee C, Tsai Y-C and Ting T-C 2019 Absorption coefficient of water vapor across atmospheric troposphere layer *Heliyon* **5** e01145
[36] Sun X, Sun Y, Zhou Z, Alam M A and Bermel P 2017 Radiative sky cooling: fundamental physics, materials, structures, and applications *Nanophotonics* **6** 997–1015
[37] NASA 2022 Prediction of worldwide energy resources (POWER) *Data Access Viewer* (available at: https://power.larc.nasa.gov/)
[38] Motlagh N H, Mohammadrezaei M, Hunt J and Zakeri B 2020 Internet of things (IoT) and the energy sector *Energies* **13** 1–27